Supplement of Atmos. Chem. Phys., 19, 6367–6388, 2019
https://doi.org/10.5194/acp-19-6367-2019-supplement


Atmospheric Chemistry and Physics
Open Access
EGU

*Supplement of*

# Inversely modeling homogeneous $H_2SO_4$-$H_2O$ nucleation rate in exhaust-related conditions

**Miska Olin et al.**

*Correspondence to:* Miska Olin (miska.olin@tuni.fi)

## 1 Comparing simulated sulfuric acid concentrations to the measured concentrations

In addition to determining sulfuric acid concentrations ($[H_2SO_4]$) through inverse modeling, they were also measured using a nitrate ion ($NO_3^-$) based chemical ionization Atmospheric Pressure interface Time-Of-Flight mass spectrometer (CI-APi-TOF, Jokinen et al. (2012)) and Ion Chromatography (IC, Sulonen et al. (2015)).

The CI-APi-TOF used $NO_3^-$ ions as reagent ions to detect $H_2SO_4$ as bisulfate ions ($HSO_4^-$) and their clusters with nitric acid ($HNO_3$) in an APi-TOF mass spectrometer (Tofwerk AG, Switzerland and Aerodyne Research Inc., USA). The CI-APi-TOF outputs the concentrations of the measured ions as counts per second ($c_{\text{ion}}$) which need to be converted to absolute $H_2SO_4$ concentrations with the equation (Tröstl et al., 2016)

$$[H_2SO_4] = C \cdot \ln\left(1 + \frac{c_{HSO_4^-} + c_{HNO_3 \cdot HSO_4^-} + c_{H_2SO_4 \cdot HSO_4^-}}{c_{NO_3^-} + c_{HNO_3 \cdot NO_3^-} + c_{(HNO_3)_2 \cdot NO_3^-}}\right), \tag{S1}$$

where $C$ is an experimentally determined calibration coefficient having the value of $1.3 \times 10^9\,\mathrm{cm}^{-3}$ for the device used. The CI-APi-TOF works well in measuring $H_2SO_4$ from the atmosphere; however, because the concentrations in this experiment were significantly higher, the raw sample needed to be diluted. The sample flow rate to the CI-APi-TOF was $(10.0 \pm 0.2)$ slpm and it was prepared by diluting the raw sample with compressed air heated to 300 °C with the flow rate of almost 10 slpm. The dilution ratio, determined using carbon dioxide ($CO_2$) measurement, was $133 \pm 7$. This corresponds to the raw sample flow rate of $(0.075 \pm 0.004)$ slpm. The length of the sampling line before the dilution point was 70 mm and between the dilution point and the inlet of the CI-APi-TOF it was 1720 mm. According to the diffusional losses (Gormley and Kennedy, 1948), only the fraction of $(6 \pm 2) \times 10^{-4}$ of $H_2SO_4$ penetrated to the CI-APi-TOF inlet, of which the major contribution resulted from the sampling line before the dilution point having a very low flow rate.

The IC measurement was performed by sucking the raw sample with the flow rate of $(2.76 \pm 0.02)$ slpm through a gas washing bottle with a fritted disc and analyzing $SO_4^{2-}$ ion concentration from the liquid sample with the IC instrument off-line. The length of the sampling line before the washing bottle was 525 mm, for which the calculated penetration due to diffusional losses is $(20.4 \pm 0.4)\,\%$. The effect of the line length on the diffusional losses was examined using also a sampling line having the length of 750 mm, for which the calculated penetration is $(12.9 \pm 0.4)\,\%$. However, according to the measured $[SO_4^{2-}]$, the line length had no effect on the penetrated fraction, implying over-predicted diffusional losses in the first part of the sampling line, probably due to saturating $H_2SO_4$ liquid onto the sampling lines. The gas washing bottle was filled with 130 ml of deionized Milli-Q water and the gas collecting time was 20 ... 360 min, depending on the expected $[H_2SO_4]$ in the raw sample. The collection efficiency of the gas washing bottle was measured by collecting the sample also with 80 ml of water having approximately half the bubbling height of 130 ml of water. According to the measured $[SO_4^{2-}]$, the amount of water had no effect on the results; thus, the collection efficiency was high, or at least the maximum achievable in the measurement conditions.

$H_2SO_4$ concentrations in the raw sample with different $H_2SO_4$ evaporator temperatures measured with the CI-APi-TOF and the IC are presented together with the simulated and theoretical concentrations in Fig. S1. Surprisingly, the CI-APi-TOF data are at a somewhat higher level compared to the lossless level which is probably partially accounted by the calculated diffusional losses between the measurement point and the device, which have a large uncertainty due to a very low sample flow rate. The reason why the data lies near the lossless level is presumably due to the direction of adjusting $T_{\text{sa}}$ which was from high to low temperatures during the CI-APi-TOF measurement and the time waited for the CI-APi-TOF signal to stabilize was short with respect to the equilibration time of the sampling line. Performing higher saturator temperatures first can saturate the walls of the sampling lines with $H_2SO_4$ which could later act as preventing diffusional losses with lower saturator temperatures and thus result into the lossless level. The IC data are at the level of about 5 % of the lossless theoretical level, but there are also significant outliers at higher levels. The level of the IC data can be lowered due to the sample containing $CO_2$. $CO_2$ can lower the pH of the liquid sample in the gas washing bottle, which can further decrease the collection efficiency of $SO_4^{2-}$. The 5 % level of the IC data and the direction of the effect of $CO_2$ would denote maximum diffusional losses onto the sampling lines between the evaporator and the $[H_2SO_4]_{\text{raw}}$ measurement point of 95 %, which lies in the range of calculated diffusional losses of 0 ... 98 %.

Nevertheless, both the measured data sets agree well with the shape of the theoretical curve, which implies that $[H_2SO_4]_{raw}$ can be estimated using $T_{sa}$. However, the absolute value for $[H_2SO_4]_{raw}$ cannot be satisfactorily estimated using neither $T_{sa}$ nor the measured concentrations due to the discrepancy of the measured concentrations. Therefore, the simulations of this study did not use the measured concentrations as the boundary conditions; instead, the $[H_2SO_4]_{raw}$ values were obtained through inverse modeling.

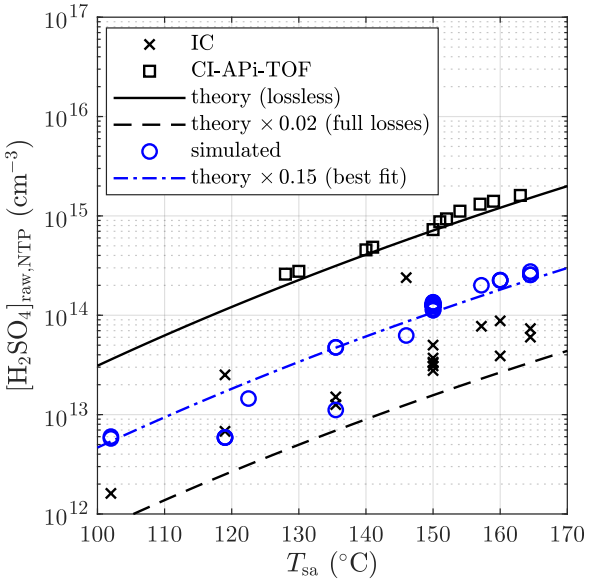


**Figure S1.** Simulated sulfuric acid concentrations in the raw sample compared to the measured and the theoretical concentrations with different sulfuric acid evaporator temperatures. The concentrations are presented as the concentrations in NTP (normal temperature and pressure) conditions rather than in a hot raw sample.

## 2 Uncertainty estimation for particle size distribution measurements

The disagreement of sub-6 nm particle size distributions measured by the combination of the PSM and the CPC 3775 and by the Nano-SMPS is examined by investigating the sources causing uncertainties to the size distributions obtained from these devices. Uncertainties associated with both the systematic and random effects in the calculated size distributions after the ejector diluter are calculated as follows.

### 2.1 Calculation of the uncertainties for the size distributions measured by the combination of the PSM and the CPC 3775

The particle number size distributions are calculated using the step-wise method according to Lehtipalo et al. (2014). Backwards-correcting the measured distributions to represent the distributions after the ejector diluter requires multiplying the data with the dilution ratio of the bridge diluter and dividing by the penetration efficiency of particles in the sampling lines between the ejector diluter and the measurement devices. Finally, the equation to obtain the distribution at particle size $D_{p,i}$ after the ejector

diluter from the measured concentrations is

$$\nu(D_{\mathrm{p},i}) = \frac{N_i^{\text{smaller}} - N_i^{\text{larger}}}{\log(D_{\mathrm{p},i}^{\text{larger}}/D_{\mathrm{p},i}^{\text{smaller}}) \cdot p(D_{\mathrm{p},i}, L/Q)} \tag{S2}$$

where $N_i^{\text{smaller}}$ and $N_i^{\text{larger}}$ are particle number concentrations measured with the $D_{50}$-cut-sizes of $D_{\mathrm{p},i}^{\text{smaller}}$ and $D_{\mathrm{p},i}^{\text{larger}}$, respectively. $D_{\mathrm{p},i}$ is the geometric mean diameter of the $D_{50}$-cut-sizes and $p(D_{\mathrm{p},i}, L/Q)$ is the penetration efficiency of particles with a diameter of $D_{\mathrm{p},i}$ in a sampling line with a length of $L_{\text{lines}} = L$ and flow rate of $Q_{\text{lines}} = Q$, according to diffusional losses calculated with the equations of Gormley and Kennedy (1948). This penetration efficiency takes also the bridge diluter into account because its operation principle is also based on diffusional losses; thus, $L$ denotes the effective length of the combined effect of the sampling lines and the bridge diluter.

Uncertainties associated with the systematic effects in the calculated size distributions after the ejector diluter include the uncertainty of the cut-diameters and the uncertainty of the value of $L/Q$. Because the detection efficiency curves of the PSM and CPC 3775 are measured using particles having a different composition than $H_2SO_4$-$H_2O$, as in these measurements, and because environmental parameters, such as temperature, can have effects on the detection efficiency curves, the reported cut-diameters may not hold exactly. The relative uncertainty of 20 % is estimated for the cut-diameters and also for the ratio of the cut-diameters $D_{\mathrm{p},i}^{\text{larger}}/D_{\mathrm{p},i}^{\text{smaller}}$ because it is expected that if one of the cut-diameters is deviated towards smaller or larger particle sizes, another one is deviated towards the same direction. 10 % relative uncertainty is estimated for the value of $L/Q$, which includes the uncertainty of the measurement of both $L$ and $Q$ and the uncertainty in the equations of Gormley and Kennedy (1948).

Uncertainties associated with the random effects arise from the noise in the measured concentrations caused by the instability of the particle generation. The relative standard deviations of the measured concentrations are in the range of 1 ... 25 %, depending on the concentration level and particle sizes: higher concentrations and larger particle sizes provided more stable particle generation compared to lower concentrations and smaller particle sizes.

The uncertainty associated with both the systematic and random effects for $\nu(D_{\mathrm{p},i})$ can be calculated with the equation

$$\begin{aligned}\frac{\Delta\nu}{\nu} &= \sqrt{\left(\frac{\partial\nu}{\partial N_i^{\text{smaller}}}\frac{\Delta N_i^{\text{smaller}}}{\nu}\right)^2 + \left(\frac{\partial\nu}{\partial N_i^{\text{larger}}}\frac{\Delta N_i^{\text{larger}}}{\nu}\right)^2 + \left(\frac{\partial\nu}{\partial\log(D_{\mathrm{p},i}^{\text{larger}}/D_{\mathrm{p},i}^{\text{smaller}})}\frac{\Delta\log(D_{\mathrm{p},i}^{\text{larger}}/D_{\mathrm{p},i}^{\text{smaller}})}{\nu}\right)^2 + \left(\frac{\partial\nu}{\partial p}\frac{\Delta p}{\nu}\right)^2} \\ &= \sqrt{\left(\frac{\Delta N_i^{\text{smaller}}}{N_i^{\text{smaller}} - N_i^{\text{larger}}}\right)^2 + \left(\frac{\Delta N_i^{\text{larger}}}{N_i^{\text{smaller}} - N_i^{\text{larger}}}\right)^2 + \left(\frac{\Delta\log(D_{\mathrm{p},i}^{\text{larger}}/D_{\mathrm{p},i}^{\text{smaller}})}{\log(D_{\mathrm{p},i}^{\text{larger}}/D_{\mathrm{p},i}^{\text{smaller}})}\right)^2 + \left(\frac{\Delta p}{p}\right)^2}\end{aligned} \tag{S3}$$

where $\Delta N_i^{\text{smaller}}$ and $\Delta N_i^{\text{smaller}}$ are the standard deviations of the measured concentrations, depending on the measurement case, the third term is $0.2^2$ because $\Delta(D_{\mathrm{p},i}^{\text{larger}}/D_{\mathrm{p},i}^{\text{smaller}})/(D_{\mathrm{p},i}^{\text{larger}}/D_{\mathrm{p},i}^{\text{smaller}}) = 20\,\%$, and $\Delta p/p$ is the relative uncertainty for $p$ depending on the particle size and is calculated with the equation

$$\frac{\Delta p}{p} = \sqrt{\left(\frac{\partial p}{\partial(L/Q)}\frac{\Delta(L/Q)}{p}\right)^2 + \left(\frac{\partial p}{\partial D_{\mathrm{p},i}}\frac{\Delta D_{\mathrm{p},i}}{p}\right)^2} \tag{S4}$$

using $\Delta(L/Q)/(L/Q) = 10\,\%$ and $\Delta D_{\mathrm{p},i}/D_{\mathrm{p},i} = 20\,\%$.

### 2.2 Calculation of the uncertainties for the size distributions measured by the Nano-SMPS

The particle number size distributions reported by the Nano-SMPS device have already went through the manufacturer's inversion algorithm. Thus, the inverse modeling of this work does not try to predict the concentration measured as a function of time measured by the CPC 3776, acting as a particle counter in the Nano-SMPS system. Instead, the inverse modeling takes only the diffusional losses in the sampling lines and the CPC 3776 detection efficiency curve into account, but not, e.g., the radioactive charger efficiency and the diffusional losses inside the device. It is partly unknown what is included in the

manufacturer's inversion algorithm, but at least the charger efficiency and the diffusional losses inside the device are included. The inversion algorithm probably includes also the CPC 3776 detection efficiency curve, $f_{\mathrm{CPC}}$, but it is, however, included in the inverse modeling of this work because it seems that it may differ significantly from the curve reported by the manufacturer, according to Hermann et al. (2007) and Mordas et al. (2008), as presented in Fig. S2. Unfortunately, the curve for the device used in these measurements is not measured; therefore, the inversion modeling uses the one reported by Mordas et al. (2008) because it lies between the other two curves, representing an average one. The uncertainty of the detection efficiency at a specific diameter is calculated from the maximum range of variation of the detection efficiencies from these three different sources.

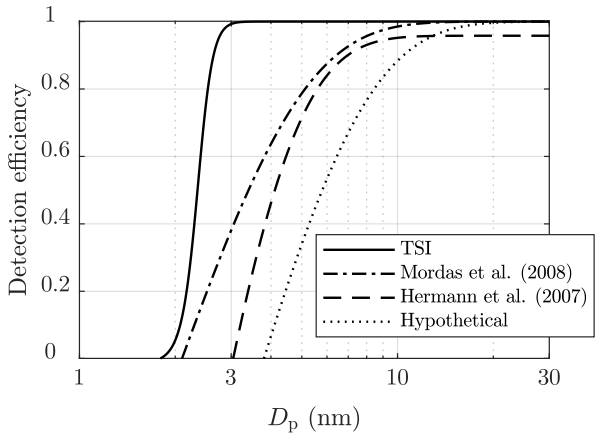


**Figure S2.** The CPC 3776 detection efficiency curves as a function of particle size reported by the manufacturer, Hermann et al. (2007), and Mordas et al. (2008). Additionally, a hypothetical curve correcting the disagreement between sub-6 nm particle size distributions measured by the Nano-SMPS and PSM+CPC system is presented.

The hypothetical detection efficiency curve presented in Fig. S2 is based on the curve reported by Mordas et al. (2008) but with different parameters. If this hypothetical curve is the actual curve of the device used, the size distributions as in Fig. 4 will be corrected to the distributions presented in Fig. S3, from which it can be seen that the size distributions measured by different devices correspond clearly better, at least for the two cases having the lowest $T_{\mathrm{sa}}$. The PSM+CPC distribution for the case having the highest $T_{\mathrm{sa}}$ is probably overestimated due to noise in the measured concentration because, according to Fig. 10 (c), the concentrations measured with different cut-diameters are on the same level, implying that there should not be a notable amount of particles in that size range.

Other uncertainties associated with the systematic effects, in addition to the uncertainty involved in the CPC 3776 detection efficiency curve, include the uncertainties of the charger efficiency, the diffusional losses correction, and the particle sizes interpreted by the manufacturer's inversion algorithm. The charger of the Nano-SMPS used was a TSI 3077 radioactive Kr-85 charger, which is based on charging particles bipolarly to the charge equilibrium state. The inversion algorithm uses the positive charge distribution function, $f_{\mathrm{charger}}$, reported by Wiedensohler (1988). It is a semi-empirical function in which the mobilities and masses of positive and negative ions in the carrier gas are fitted based on the charge distribution measurements (Hussin et al., 1983; Adachi et al., 1985; Wiedensohler et al., 1986) made for particles larger than 5 nm in diameters. Alonso et al. (1997) have measured the charge distributions down to particle diameters of 2.5 nm. Unfortunately, the charger distributions from all these measurements differ, especially for the smallest particle sizes, and have thus different ion parameters, due to different particle compositions, carrier gas compositions, and the accuracies of the particle size measurements. Therefore, the charger efficiency function selected in the manufacturer's inversion algorithm may not be very accurate. Based on the differences between the results of these charge distribution measurements, the relative uncertainties of 30, 20, and 10 % for the charger efficiencies at particle diameters of 6, 10, and 20 nm, respectively, are estimated. Another factor causing uncertainty for the charger efficiency is how satisfactorily the charge distribution is developed to the equilibrium state. If the residence

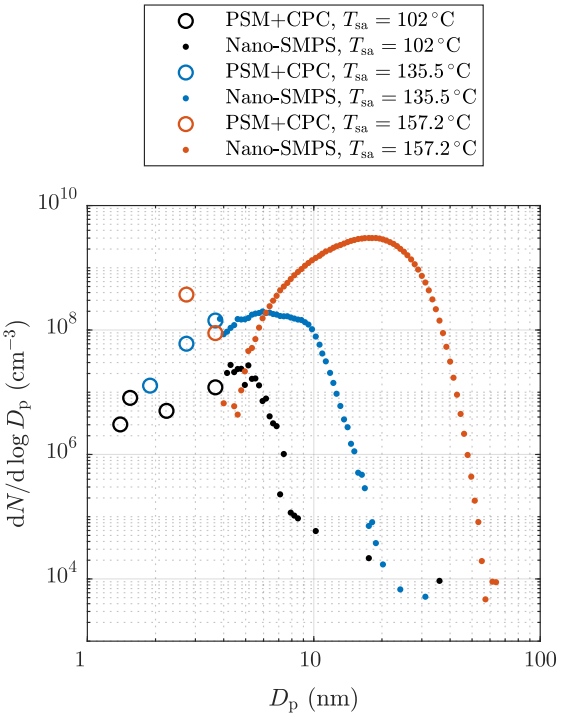


**Figure S3.** The corrected particle size distributions as in Fig. 4 if the detection efficiency curve of the CPC 3776 would be the hypothetical curve presented in Fig. S2.

time inside the charger is too short (Alonso et al., 1997), the activity of the charger is too low (de La Verpilliere et al., 2015) (e.g, if the activity of the charger is depleted due to a long operating life), or if the particle concentration is too high compared to the ion concentration (Wiedensohler et al., 2012), the equilibrium state may not be reached and the charger efficiency is overestimated. According to the deviations of the charge distributions in the measurements of de La Verpilliere et al. (2015) from the charge distribution function of Wiedensohler (1988), the relative uncertainties of 40, 30, and 20 % for the charger efficiencies at particle diameters of 2, 6, and 10 nm, respectively, are estimated. Because the particles before the Nano-SMPS are supposedly uncharged in this work, the possible incomplete reaching of the charge equilibrium state causes that the particles are less charged than predicted. Therefore, the concentrations would be underestimated, and thus the possible error related to this is considered only negative.

The diffusional losses of the particles in the sampling lines of this work are based on the equations of Gormley and Kennedy (1948) using the $L_{\mathrm{lines}}/Q_{\mathrm{lines}}$ parameter as in the case of the PSM+CPC system (the relative uncertainty of 10 % for the $L_{\mathrm{lines}}/Q_{\mathrm{lines}}$ parameter in this case is again estimated). The correction of the diffusional losses inside the Nano-SMPS device is also based on those equations in the manufacturer's inversion algorithm. The algorithm uses an empirically fitted $L_{\mathrm{device}}/Q_{\mathrm{device}}$ value which included the whole route of the particles inside the device even though the route is not a perfect laminar circular tube flow, for which the analytical solution by Gormley and Kennedy (1948) is based on. Therefore, the penetration function for particles inside the device, $p_{\mathrm{device}}$, may not be very accurate and the relative uncertainty of 10 % for the $L_{\mathrm{device}}/Q_{\mathrm{device}}$ parameter is estimated.

The correction factor assumed to exist in the inversion algorithm of the Nano-SMPS, to which the penetration in the sampling lines, $p_{\mathrm{lines}}$, is added, is

$$C(D_{\mathrm{p},i}) = \frac{1}{f_{\mathrm{charger}}(D_{\mathrm{p},i}) \cdot f_{\mathrm{CPC}}(D_{\mathrm{p},i}) \cdot p_{\mathrm{device}}(D_{\mathrm{p},i}, L_{\mathrm{device}}/Q_{\mathrm{device}}) \cdot p_{\mathrm{lines}}(D_{\mathrm{p},i}, L_{\mathrm{lines}}/Q_{\mathrm{lines}})}. \tag{S5}$$

The concentration measured with a specific DMA (Differential Mobility Analyzer) voltage at a specific time, related to the particle diameter of $D_{\mathrm{p},i}$ (obtained though the inversion algorithm), is multiplied with $C(D_{\mathrm{p},i})$ in order to obtain the size distribution in a location of $L_{\mathrm{lines}}$ before the device, i.e., after the ejector diluter in this case. For very small particles, all the four functions in Eq. (S5) have very low value; and thus, the value of $C(D_{\mathrm{p},i})$ is extremely high. This is illustrated in Fig. S4 from which it can be observed that the value for sub-6 nm particles is several orders of magnitude. Very high correction factor denotes very low number of particle counts detected by the CPC at a specific diameter, and very low counts do not provide good precision due to statistics: there may be only a few randomly detected single particles or there may be even not a single detection at all during the time dedicated to that particle size, even though multiple scans have been performed for one measurement case. In the case of no or very low detection of single particles, uncertainties cannot be calculated. Because the correction factor increases very steeply with decreasing particle size, the uncertainties involved in the functions in Eq. (S5) can deviate it in high extent. Another consequence of the steep behavior of the correction factor is that if there is even a minor error in the interpreted particle diameters, the value of the correction factor can be significantly misestimated. There are several factors that can cause error to the particle diameters measured by the Nano-SMPS (Wiedensohler et al., 2012); here, the relative uncertainty of 5 % is estimated for the diameters.

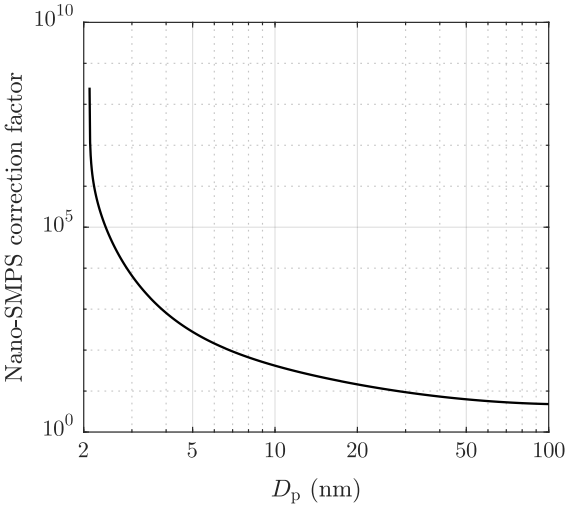


**Figure S4.** Nano-SMPS correction factor, as in Eq. (S5), used to correct the measured particle concentrations in the data inversion.

The uncertainty associated with both the systematic and random effects for the size distributions, $\nu(D_{\mathrm{p},i})$, can be calculated with the equation

$$\frac{\Delta\nu}{\nu} = \sqrt{\left(\frac{\Delta\nu'}{\nu'}\right)^2 + \left(\frac{\Delta C}{C}\right)^2} \tag{S6}$$

where $\Delta\nu'/\nu'$ is the relative standard deviation of the size distributions at the particle diameter of $D_{\mathrm{p},i}$ output by the device and $\Delta C/C$ is the relative uncertainty of the Nano-SMPS correction factor. $\Delta\nu'/\nu'$ represents uncertainties associated with the random effects arisen from the noise in the measured concentrations caused by the instability of the particle generation, as in the case of the PSM+CPC system, but also from low precision in measuring particles sizes having a very low overall detection

efficiency and particle sizes having low concentration in the measured case. $\Delta C/C$ is calculated with the equation

$$\begin{aligned}\frac{\Delta C}{C} &= \sqrt{\left(\frac{\partial C}{\partial f_{\text{charger}}}\frac{\Delta f_{\text{charger}}}{C}\right)^2 + \left(\frac{\partial C}{\partial f_{\text{CPC}}}\frac{\Delta f_{\text{CPC}}}{C}\right)^2 + \left(\frac{\partial C}{\partial p_{\text{device}}}\frac{\Delta p_{\text{device}}}{C}\right)^2 + \left(\frac{\partial C}{\partial p_{\text{lines}}}\frac{\Delta p_{\text{lines}}}{C}\right)^2 + \left(\frac{\partial C}{\partial D_{\text{p},i}}\frac{\Delta D_{\text{p},i}}{C}\right)^2} \\ &= \sqrt{\left(\frac{\Delta f_{\text{charger}}}{f_{\text{charger}}}\right)^2 + \left(\frac{\Delta f_{\text{CPC}}}{f_{\text{CPC}}}\right)^2 + \left(\frac{\Delta p_{\text{device}}}{p_{\text{device}}}\right)^2 + \left(\frac{\Delta p_{\text{lines}}}{p_{\text{lines}}}\right)^2 + \left(\frac{\partial C}{\partial D_{\text{p},i}}\frac{\Delta D_{\text{p},i}}{C}\right)^2}\end{aligned} \tag{S7}$$

where $\Delta f_{\text{charger}}/f_{\text{charger}}$ and $\Delta f_{\text{CPC}}/f_{\text{CPC}}$ are the relative uncertainties for $f_{\text{charger}}$ and $f_{\text{CPC}}$ having the values mentioned before, $\Delta p_{\text{device}}/p_{\text{device}}$ and $\Delta p_{\text{lines}}/p_{\text{lines}}$ are the relative uncertainties for the penetration efficiencies, $p_{\text{device}}$ and $p_{\text{lines}}$, and the last term represents the relative uncertainty of $C$ caused by the uncertainty of particle diameters. $\Delta p_{\text{device}}/p_{\text{device}}$ and $\Delta p_{\text{lines}}/p_{\text{lines}}$ depend on the particle diameter and are calculated with the equations

$$\begin{aligned}\frac{\Delta p_{\text{device}}}{p_{\text{device}}} &= \frac{\partial p_{\text{device}}}{\partial(L_{\text{device}}/Q_{\text{device}})}\cdot\frac{\Delta(L_{\text{device}}/Q_{\text{device}})}{p_{\text{device}}} \\ \frac{\Delta p_{\text{lines}}}{p_{\text{lines}}} &= \frac{\partial p_{\text{lines}}}{\partial(L_{\text{lines}}/Q_{\text{lines}})}\cdot\frac{\Delta(L_{\text{lines}}/Q_{\text{lines}})}{p_{\text{lines}}}\end{aligned} \tag{S8}$$

which differ from Eg. (S4) by missing the effect of the particle diameter because that effect is included in the last term of Eq. (S7). The last term represents the total effect of the uncertainty of particle diameter on the uncertainty of $C$ because particle diameter is involved in all the other four terms.

### 2.3 Calculated uncertainties for the size distributions

The relative uncertainties for the size distributions between 2 and 10 nm after the ejector diluter caused by the uncertainties associated with the different effects involved in the size distribution measurements are presented in Tab. S1. For the PSM+CPC system, the most significant relative uncertainties associated with the systematic effects arise from the uncertainty of the cut-diameters (12 ... 30 %), partly due to correcting the diffusional losses in sampling lines needed in backwards-correcting the measured distributions to represent the distributions after the ejector diluter. For the Nano-SMPS, the uncertainty of the charger efficiency plays a major role in the relative uncertainties associated with the systematic effects (40 ... 66 %), but the uncertainty of the CPC 3776 detection efficiency curve has also a significant role for the smallest particles (55 % for 3.7 nm). The relative uncertainties decrease steeply when measuring particles sized 10 nm or larger using the Nano-SMPS. Both devices are, in theory, capable in measuring the size distribution at 3.7 nm, but the uncertainties with the Nano-SMPS are clearly higher compared to the PSM+CPC system. Therefore, the PSM+CPC system suits better in measuring near that diameter.

Uncertainties associated with the random effects caused by the noise in the measured concentrations due to instability in particle generation for the both devices and by low counting statistics of the Nano-SMPS also have significant effects if there is not a notable amount of concentration in a specific size range. In the case with $D_{\bar{m}} = 3.6\,\text{nm}$, there is a notable amount of concentration in the PSM+CPC size range, and thus, the relative uncertainties are relatively low (22 ... 61 %) for the PSM+CPC system. For the Nano-SMPS, the relative standard deviation of the size distribution for the 6 nm particles is 72 %, which is, however, the particle size measured with the highest precision in that case: larger particles are inexistent and smaller particles are not detected. In the case with $D_{\bar{m}} = 19\,\text{nm}$, the Nano-SMPS suits well in measuring the size distribution at the particle size of 10 nm (the relative standard deviation of 10 % originating mainly from the instability in the particle generation) and also relatively well at the particle size of 6 nm (the relative standard deviation of 24 %), but the uncertainties increase with the particles smaller than 6 nm. Conversely, the PSM+CPC system has high uncertainties because the concentration in the PSM+CPC size range is so low that the difference between the concentrations measured with different cut-diameters are smaller than the standard deviation of the concentrations (see Fig. 10), which is always a problem with the PSM having a cumulative nature in measuring concentrations, if the cut-diameters of the adjacent saturator flow rates are too near or the measured signal is too unstable. This issue can be overcome by skipping the data measured with the adjacent cut-diameters or even by considering only the data measured with the smallest and with the largest cut-diameter. However, while the precision will be higher in this alternative method, the information on the shape of the size distribution in that size range will diminish.

**Table S1.** The relative uncertainties (in percents) for the size distributions after the ejector diluter, $\Delta\nu/\nu$ (%), for the selected particle diameters. The first seven lines represent the relative uncertainties associated with the systematic effects and are thus independent of the measurement cases. The last two lines represent the relative uncertainties associated with the random effects for two selected measurement cases having small and large particles.

| Device | PSM+CPC | | Nano-SMPS | | |
|---|---|---|---|---|---|
| $D_\mathrm{p}$ | 2 nm | 3.7 nm | 3.7 nm | 6 nm | 10 nm |
| Diffusional losses in sampling lines $\left(\frac{\Delta(L_\mathrm{lines}/Q_\mathrm{lines})}{L_\mathrm{lines}/Q_\mathrm{lines}} = 10\,\%\right)$ | 8 | 3 | 4 | 2 | 1 |
| Diffusional losses in sampling lines $\left(\frac{\Delta D_{\mathrm{p},i}}{D_{\mathrm{p},i}} = 20\,\%\right)$ | 30 | 12 | | | |
| PSM detection efficiency $\left(\frac{\Delta(D_{\mathrm{p},i}^\mathrm{larger}/D_{\mathrm{p},i}^\mathrm{smaller})}{D_{\mathrm{p},i}^\mathrm{larger}/D_{\mathrm{p},i}^\mathrm{smaller}} = 20\,\%\right)$ | 20 | 20 | | | |
| Kr-85 charger efficiency | | | 66 | 61 | 40 |
| CPC 3776 detection efficiency | | | 55 | 8 | 0.7 |
| Diffusional losses inside the DMA $\left(\frac{\Delta(L_\mathrm{lines}/Q_\mathrm{lines})}{L_\mathrm{lines}/Q_\mathrm{lines}} = 10\,\%\right)$ | | | 16 | 7 | 3 |
| Nano-SMPS correction factor $\left(\frac{\Delta D_{\mathrm{p},i}}{D_{\mathrm{p},i}} = 5\,\%\right)$ | | | 32 | 17 | 10 |
| Random effects in $D_{\bar{m}} = 3.6\,\mathrm{nm}$ case (102 °C) | 61 | 22 | –[a] | 72 | –[a] |
| Ramdom effects in $D_{\bar{m}} = 19\,\mathrm{nm}$ case (157.2 °C) | $\infty$[b] | 250 | –[a] | 24 | 10 |

[a] Cannot be calculated due to insufficient particle counts.
[b] For this point, $\nu(2\,\mathrm{nm}) = 0$ but $\Delta\nu$ is a non-zero number due to the standard deviations of $N_i^\mathrm{smaller}$ and $N_i^\mathrm{smaller}$.

The error bars representing the uncertainties associated with both the systematic and random effects for the size distributions shown in Fig. 4 are presented in Fig. S5. By considering the error bars, the distributions from the both devices agree for the cases in panes (a) and (c), whereas the case in pane (b) has still some disagreement implying that other sources of uncertainty than accounted here can be involved in the measurements using these devices. According to the error bars near the particle size of 4 nm connecting the two size distributions, the PSM+CPC system provides more reliable results in the cases in panes (a) and (b). Conversely, in the case in pane (c), the Nano-SMPS provides more reliable results because, although there are two points in the PSM+CPC distribution, the alternative method shows no particles at all. However, the error bars for the alternative method are high; thus, the existence of particles in the PSM+CPC size range is still probable. Nevertheless, the fraction of particles in that size range compared to the total particle count is, definitely, some orders of magnitude smaller than in the cases in panes (a) and (b). The distributions and their uncertainties near the particle size of 4 nm, where the distributions from the both devices are available, are decided to keep separated here due to high systematic error possible in the Nano-SMPS data, although by combining the distributions would cause lower overall uncertainties. Figure S6 presents the error bars for the distributions shown in Fig. 11.

In conclusion, the reliability of our Nano-SMPS system was low for the particle sizes smaller than ∼10 nm, for the most part due to the uncertainties involved in the radioactive charger efficiency and the CPC 3776 detection efficiency. Wiedensohler et al. (2012) have performed an intercomparison of several mobility particle sizers, in which the different devices provided a good agreement for the particle sizes larger than ∼15 nm but had significant disagreements for the smaller particle sizes, without explanation. Due to the difficulties that the Nano-SMPS has in determining the size distribution reliably in sub-10 nm diameter range, in the cases studied here and elsewhere, we found that the PSM+CPC system was better suited in determining the size distribution in that particle size range, or at least in determining the total number concentration of particles larger than ∼1 nm.

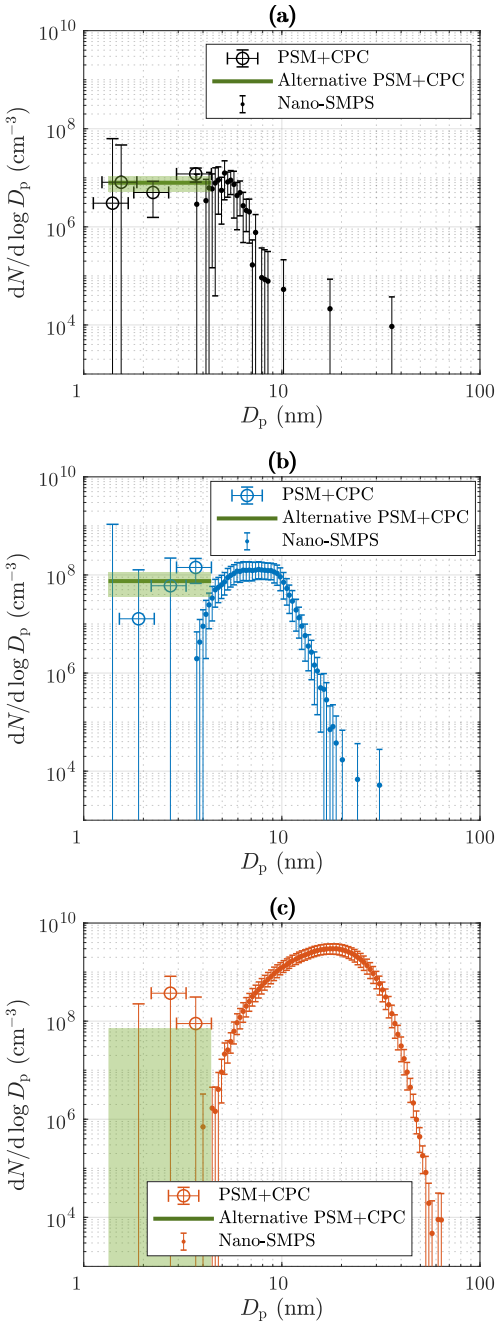


**Figure S5.** The measured size distributions for the measurement cases having the $T_{\mathrm{sa}}$ of (a) 102 °C, (b) 135.5 °C, and (c) 157.2 °C, as shown in Fig. 4, with the error bars representing the uncertainties associated with both the systematic and random effects. The alternative PSM+CPC distributions represent the distributions using only the concentrations measured with the smallest and the largest cut-diameters, in order to increase the precision. The green shaded areas denote the error bars for the distributions from the alternative method. The error bars for the particle sizes obtained from the Nano-SMPS (±5 %) are not shown for clarity.

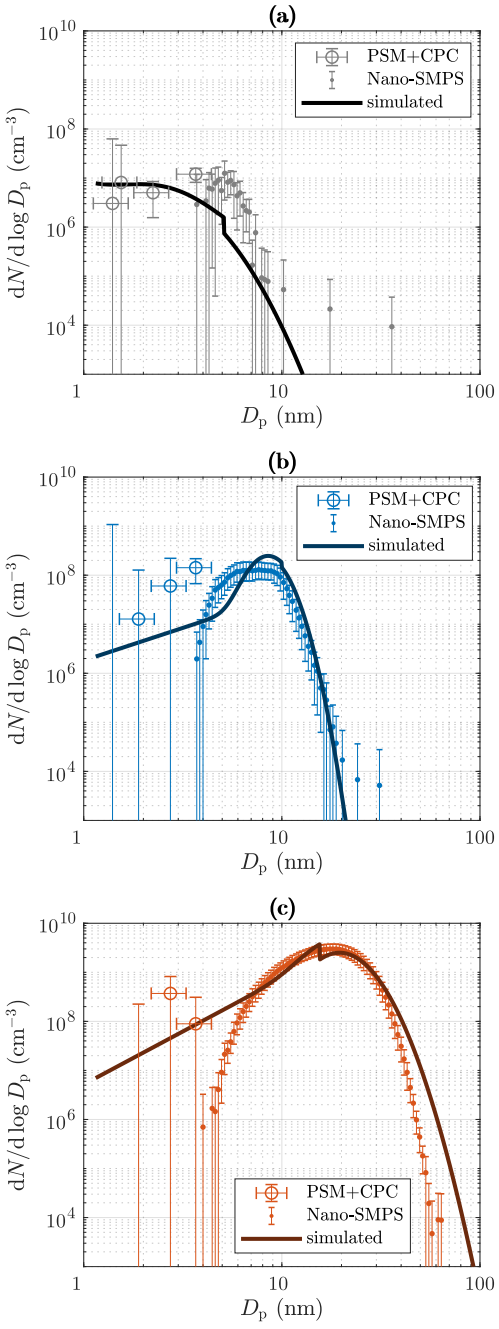


**Figure S6.** The simulated and measured size distributions for the measurement cases having the $T_{\mathrm{sa}}$ of (a) 102 °C, (b) 135.5 °C, and (c) 157.2 °C, as shown in Fig. 11, with the error bars representing the uncertainties associated with both the systematic and random effects. The error bars for the particle sizes obtained from the Nano-SMPS (±5 %) are not shown for clarity.

### 2.4 Calculation of the uncertainties for the diameters with the average mass

The diameter with the average mass of a distribution is calculated by

$$D_{\bar{m}} = \left(\frac{M'}{N}\right)^{\frac{1}{3}} = \left(\frac{\sum_i^{\mathrm{PC}} \nu(D_{\mathrm{p},i}) \cdot \mathrm{d}\log D_{\mathrm{p},i} \cdot D_{\mathrm{p},i}^3 + \sum_i^{\mathrm{NS}} \nu(D_{\mathrm{p},i}) \cdot \mathrm{d}\log D_{\mathrm{p},i} \cdot D_{\mathrm{p},i}^3}{\sum_i \nu(D_{\mathrm{p},i}) \cdot \mathrm{d}\log D_{\mathrm{p},i}}\right)^{\frac{1}{3}} = \left(\frac{M'_{\mathrm{PC}} + M'_{\mathrm{NS}}}{N}\right)^{\frac{1}{3}} \tag{S9}$$

where $M'$ is the third moment of the distribution, $M'_{\mathrm{PC}}$ and $M'_{\mathrm{NS}}$ are the parts of the third moment from the PSM+CPC data and from the Nano-SMPS data, respectively, and $N$ is the total number concentration.

The relative uncertainty for $D_{\bar{m}}$ can be calculated with the equation

$$\frac{\Delta D_{\bar{m}}}{D_{\bar{m}}} = \sqrt{\left(\frac{\Delta D_{\bar{m}}}{D_{\bar{m}}}\bigg|_{\Delta D_{\mathrm{p}}}\right)^2 + \left(\frac{\Delta D_{\bar{m}}}{D_{\bar{m}}}\bigg|_{\Delta \nu_{\mathrm{s}}}\right)^2 + \left(\frac{\Delta D_{\bar{m}}}{D_{\bar{m}}}\bigg|_{\Delta \nu_{\mathrm{r}}}\right)^2} \tag{S10}$$

where the first term represents the relative uncertainty caused by the uncertainty of the interpreted particle diameters, the second term the relative uncertainty caused by the uncertainty associated with the systematic effects for the number size distribution, and the last term the relative uncertainty caused by the uncertainty associated with the random effects for the number size distribution.

The first term in Eq. (S10) is separated to the effects of the PSM+CPC system and of the Nano-SMPS, respectively:

$$\frac{\Delta D_{\bar{m}}}{D_{\bar{m}}}\bigg|_{\Delta D_{\mathrm{p}}} = \sqrt{\left(\frac{\Delta D_{\bar{m}}}{D_{\bar{m}}}\bigg|_{\Delta D_{\mathrm{p,PC_1}}}\right)^2 + \left(\frac{\Delta D_{\bar{m}}}{D_{\bar{m}}}\bigg|_{\Delta D_{\mathrm{p,NS_1}}}\right)^2}. \tag{S11}$$

Because particle diameters are dependent variables for a specific device, i.e., if one diameter is shifted to a direction, other diameters are most probably shifted to the same direction and with almost the same magnitude, the diameters in Eq. (S9) are separated to dependent and independent parts:

$$\begin{aligned} D_{\mathrm{p},i} &= D_{\mathrm{p,PC_1}} \cdot D'_{\mathrm{p},i} \\ D_{\mathrm{p},i} &= D_{\mathrm{p,NS_1}} \cdot D'_{\mathrm{p},i}. \end{aligned} \tag{S12}$$

where $D_{\mathrm{p,PC_1}}$ and $D_{\mathrm{p,NS_1}}$ denote the smallest diameters measured by the PSM+CPC system and by the Nano-SMPS, respectively, and $D'_{\mathrm{p},i}$ is a dimensionless variable denoting the ratios of all other diameters to the smallest diameter. Hence, the third moments can be expressed as

$$\begin{aligned} M'_{\mathrm{PC}} &= \sum_i^{\mathrm{PC}} \nu(D_{\mathrm{p},i}) \cdot \mathrm{d}\log D_{\mathrm{p},i} \cdot D_{\mathrm{p},i}^3 = \sum_i^{\mathrm{PC}} \nu(D_{\mathrm{p},i}) \cdot \mathrm{d}\log D_{\mathrm{p},i} \cdot (D_{\mathrm{p,PC_1}} \cdot D'_{\mathrm{p},i})^3 = D_{\mathrm{p,PC_1}}^3 \cdot \sum_i^{\mathrm{PC}} \nu(D_{\mathrm{p},i}) \cdot \mathrm{d}\log D_{\mathrm{p},i} \cdot D'^3_{\mathrm{p},i} \\ M'_{\mathrm{NS}} &= \sum_i^{\mathrm{NS}} \nu(D_{\mathrm{p},i}) \cdot \mathrm{d}\log D_{\mathrm{p},i} \cdot D_{\mathrm{p},i}^3 = \sum_i^{\mathrm{NS}} \nu(D_{\mathrm{p},i}) \cdot \mathrm{d}\log D_{\mathrm{p},i} \cdot (D_{\mathrm{p,NS_1}} \cdot D'_{\mathrm{p},i})^3 = D_{\mathrm{p,NS_1}}^3 \cdot \sum_i^{\mathrm{NS}} \nu(D_{\mathrm{p},i}) \cdot \mathrm{d}\log D_{\mathrm{p},i} \cdot D'^3_{\mathrm{p},i}. \end{aligned} \tag{S13}$$

The relative uncertainties in Eq. (S11) can now be calculated by

$$\begin{aligned} \frac{\Delta D_{\bar{m}}}{D_{\bar{m}}}\bigg|_{\Delta D_{\mathrm{p,PC_1}}} &= \frac{\partial D_{\bar{m}}}{\partial D_{\mathrm{p,PC_1}}} \cdot \frac{\Delta D_{\mathrm{p,PC_1}}}{D_{\bar{m}}} = \frac{1}{3}\frac{D_{\bar{m}}}{M'} \cdot \frac{\partial M'_{\mathrm{PC}}}{\partial D_{\mathrm{p,PC_1}}} \cdot \frac{\Delta D_{\mathrm{p,PC_1}}}{D_{\bar{m}}} = \frac{M'_{\mathrm{PC}}}{M'} \cdot \frac{\Delta D_{\mathrm{p,PC_1}}}{D_{\mathrm{p,PC_1}}} \\ \frac{\Delta D_{\bar{m}}}{D_{\bar{m}}}\bigg|_{\Delta D_{\mathrm{p,NS_1}}} &= \frac{\partial D_{\bar{m}}}{\partial D_{\mathrm{p,NS_1}}} \cdot \frac{\Delta D_{\mathrm{p,NS_1}}}{D_{\bar{m}}} = \frac{1}{3}\frac{D_{\bar{m}}}{M'} \cdot \frac{\partial M'_{\mathrm{NS}}}{\partial D_{\mathrm{p,NS_1}}} \cdot \frac{\Delta D_{\mathrm{p,NS_1}}}{D_{\bar{m}}} = \frac{M'_{\mathrm{NS}}}{M'} \cdot \frac{\Delta D_{\mathrm{p,NS_1}}}{D_{\mathrm{p,NS_1}}}. \end{aligned} \tag{S14}$$

As 20 and 5 % relative uncertainties for the diameters for the PSM+CPC system and for the Nano-SMPS, respectively, were estimated, Eq. (S11) becomes

$$\left.\frac{\Delta D_{\bar{m}}}{D_{\bar{m}}}\right|_{\Delta D_\mathrm{p}} = \frac{1}{M'}\sqrt{\left(M'_\mathrm{PC}\cdot 0.2\right)^2 + \left(M'_\mathrm{NS}\cdot 0.05\right)^2}. \tag{S15}$$

The relative uncertainties associated with the systematic and random effects are separated in the last two terms in Eq. (S10) because the possible errors due to the systematic effects for all size bins are presumably to the same direction and in almost of the same magnitude and the possible errors due to the random effects are randomly directed between different size bins because they are measured at different times. The number size distributions can be separated to the parts involving the sources of uncertainties associated with the systematic ($\Delta\nu_\mathrm{s}$) and with the random ($\Delta\nu_\mathrm{r}$) effects, respectively, using $\nu = \nu_\mathrm{s}\cdot\nu_\mathrm{r}$. The systematic effects for the uncertainty of $\nu_\mathrm{s}$ involve independent variables between the different devices, but dependent variables between the different size bins of a specific device. Hence, the second term in Eq. (S10) is further separated to the PSM+CPC system and to the Nano-SMPS, respectively, using

$$\begin{aligned}\left.\frac{\Delta D_{\bar{m}}}{D_{\bar{m}}}\right|_{\Delta\nu_\mathrm{s}} &= \sqrt{\left(\left.\frac{\Delta D_{\bar{m}}}{D_{\bar{m}}}\right|_{\Delta\nu_{\mathrm{s,PC}}}\right)^2 + \left(\left.\frac{\Delta D_{\bar{m}}}{D_{\bar{m}}}\right|_{\Delta\nu_{\mathrm{s,NS}}}\right)^2} \\ &= \sqrt{\left[\frac{D_{\bar{m}}\left(\nu+\Delta\nu_{\mathrm{s,PC}}\right) - D_{\bar{m}}\left(\nu-\Delta\nu_{\mathrm{s,PC}}\right)}{2D_{\bar{m}}}\right]^2 + \left[\frac{D_{\bar{m}}\left(\nu+\Delta\nu_{\mathrm{s,NS}}\right) - D_{\bar{m}}\left(\nu-\Delta\nu_{\mathrm{s,NS}}\right)}{2D_{\bar{m}}}\right]^2}.\end{aligned} \tag{S16}$$

The last term in Eq. (S10), related to the relative uncertainties associated with the random effects, is calculated by

$$\begin{aligned}\left.\frac{\Delta D_{\bar{m}}}{D_{\bar{m}}}\right|_{\Delta\nu_\mathrm{r}} &= \sqrt{\sum_i\left[\frac{\partial D_{\bar{m}}}{\partial\nu_\mathrm{r}(D_{\mathrm{p},i})}\cdot\frac{\Delta\nu_\mathrm{r}(D_{\mathrm{p},i})}{D_{\bar{m}}}\right]^2} = \sqrt{\sum_i\left[\left(\frac{1}{3M'}\frac{\partial M'}{\partial\nu_\mathrm{r}(D_{\mathrm{p},i})} - \frac{1}{3N}\frac{\partial N}{\partial\nu_\mathrm{r}(D_{\mathrm{p},i})}\right)\Delta\nu_\mathrm{r}(D_{\mathrm{p},i})\right]^2} \\ &= \frac{1}{3}\sqrt{\sum_i\left[\left(\frac{\mathrm{d}\log D_{\mathrm{p},i}\cdot D_{\mathrm{p},i}^3}{M'} - \frac{\mathrm{d}\log D_{\mathrm{p},i}}{N}\right)\Delta\nu_\mathrm{r}(D_{\mathrm{p},i})\right]^2}.\end{aligned} \tag{S17}$$

The calculated error bars representing the uncertainties associated with both the systematic and random effects for the diameters with the average mass are presented in Fig. 13.

## References


Adachi, M., Kousaka, Y., and Okuyama, K.: Unipolar and bipolar diffusion charging of ultrafine aerosol particles, J. Aerosol Sci., 16, 109 – 123, https://doi.org/https://doi.org/10.1016/0021-8502(85)90079-5, http://www.sciencedirect.com/science/article/pii/0021850285900795, 1985.

Alonso, M., Kousaka, Y., Nomura, T., Hashimoto, N., and Hashimoto, T.: Bipolar charging and neutralization of nanometer-sized aerosol particles, J. Aerosol Sci., 28, 1479 – 1490, https://doi.org/https://doi.org/10.1016/S0021-8502(97)00036-0, http://www.sciencedirect.com/science/article/pii/S0021850297000360, 1997.

de La Verpilliere, J. L., Swanson, J. J., and Boies, A. M.: Unsteady bipolar diffusion charging in aerosol neutralisers: A non-dimensional approach to predict charge distribution equilibrium behaviour, J. Aerosol Sci., 86, 55 – 68, https://doi.org/https://doi.org/10.1016/j.jaerosci.2015.03.006, http://www.sciencedirect.com/science/article/pii/S0021850215000440, 2015.

Gormley, P. G. and Kennedy, M.: Diffusion from a Stream Flowing through a Cylindrical Tube, P. Roy. Irish Acad. A, 52, 163–169, https://doi.org/10.2307/20488498, 1948.

Hermann, M., Wehner, B., Bischof, O., Han, H.-S., Krinke, T., Liu, W., Zerrath, A., and Wiedensohler, A.: Particle counting efficiencies of new TSI condensation particle counters, J. Aerosol Sci., 38, 674 – 682, https://doi.org/https://doi.org/10.1016/j.jaerosci.2007.05.001, http://www.sciencedirect.com/science/article/pii/S0021850207000705, 2007.

Hussin, A., Scheibel, H., Becker, K., and Porstendörfer, J.: Bipolar diffusion charging of aerosol particles—I: experimental results within the diameter range 4–30 nm, J. Aerosol Sci., 14, 671 – 677, https://doi.org/https://doi.org/10.1016/0021-8502(83)90071-X, http://www.sciencedirect.com/science/article/pii/002185028390071X, 1983.

Jokinen, T., Sipilä, M., Junninen, H., Ehn, M., Lönn, G., Hakala, J., Petäjä, T., Mauldin III, R. L., Kulmala, M., and Worsnop, D. R.: Atmospheric sulphuric acid and neutral cluster measurements using CI-APi-TOF, Atmos. Chem. Phys., 12, 4117–4125, https://doi.org/10.5194/acp-12-4117-2012, 2012.

Lehtipalo, K., Leppä, J., Kontkanen, J., Kangasluoma, J., Franchin, A., Wimmer, D., Schobesberger, S., Junninen, H., Petäjä, T., Sipilä, M., Mikkilä, J., Vanhanen, J., Worsnop, D., and Kulmala, M.: Methods for determining particle size distribution and growth rates between 1 and 3 nm using the Particle Size Magnifier, Bor. Env. Res., 19, 215–236, https://doi.org/10.1029/2001JD001010, 2014.

Mordas, G., Manninen, H., Petäjä, T., Aalto, P., Hämeri, K., and Kulmala, M.: On operation of the ultra-fine water-based CPC TSI 3786 and comparison with other TSI models (TSI 3776, TSI 3772, TSI 3025, TSI 3010, TSI 3007), Aerosol Sci. Tech., 42, 152–158, https://doi.org/10.1080/02786820701846252, 2008.

Sulonen, M. L., Kokko, M. E., Lakaniemi, A.-M., and Puhakka, J. A.: Electricity generation from tetrathionate in microbial fuel cells by acidophiles, J. Hazard. Mater., 284, 182–189, https://doi.org/10.1016/j.jhazmat.2014.10.045, 2015.

Tröstl, J., Chuang, W. K., Gordon, H., Heinritzi, M., Yan, C., Molteni, U., Ahlm, L., Frege, C., Bianchi, F., Wagner, R., Simon, M., Lehtipalo, K., Williamson, C., Craven, J. S., Duplissy, J., Adamov, A., Almeida, J., Bernhammer, A.-K., Breitenlechner, M., Brilke, S., Dias, A., Ehrhart, S., Flagan, R. C., Franchin, A., Fuchs, C., Guida, R., Gysel, M., Hansel, A., Hoyle, C. R., Jokinen, T., Junninen, H., Kangasluoma, J., Keskinen, H., Kim, J., Krapf, M., Kürten, A., Laaksonen, A., Lawler, M., Leiminger, M., Mathot, S., Möhler, O., Nieminen, T., Onnela, A., Petäjä, T., Piel, F. M., Miettinen, P., Rissanen, M. P., Rondo, L., Sarnela, N., Schobesberger, S., Sengupta, K., Sipilä, M., Smith, J. N., Steiner, G., Tomè, A., Virtanen, A., Wagner, A. C., Weingartner, E., Wimmer, D., Winkler, P. M., Ye, P., Carslaw, K. S., Curtius, J., Dommen, J., Kirkby, J., Kulmala, M., Riipinen, I., Worsnop, D. R., Donahue, N. M., and Baltensperger, U.: The role of low-volatility organic compounds in initial particle growth in the atmosphere, Nature, 533, 527–531, https://doi.org/10.1038/nature18271, 2016.

Wiedensohler, A.: An approximation of the bipolar charge distribution for particles in the submicron size range, J. Aerosol Sci., 19, 387 – 389, https://doi.org/https://doi.org/10.1016/0021-8502(88)90278-9, http://www.sciencedirect.com/science/article/pii/0021850288902789, 1988.

Wiedensohler, A., Lütkemeier, E., Feldpausch, M., and Helsper, C.: Investigation of the bipolar charge distribution at various gas conditions, J. Aerosol Sci., 17, 413 – 416, https://doi.org/https://doi.org/10.1016/0021-8502(86)90118-7, http://www.sciencedirect.com/science/article/pii/0021850286901187, 1986.

Wiedensohler, A., Birmili, W., Nowak, A., Sonntag, A., Weinhold, K., Merkel, M., Wehner, B., Tuch, T., Pfeifer, S., Fiebig, M., Fjäraa, A. M., Asmi, E., Sellegri, K., Depuy, R., Venzac, H., Villani, P., Laj, P., Aalto, P., Ogren, J. A., Swietlicki, E., Williams, P., Roldin, P., Quincey, P., Hüglin, C., Fierz-Schmidhauser, R., Gysel, M., Weingartner, E., Riccobono, F., Santos, S., Grüning, C., Faloon, K., Beddows, D., Harrison, R., Monahan, C., Jennings, S. G., O'Dowd, C. D., Marinoni, A., Horn, H.-G., Keck, L., Jiang, J., Scheckman, J., McMurry, P. H., Deng, Z., Zhao, C. S., Moerman, M., Henzing, B., de Leeuw, G., Löschau, G., and Bastian, S.: Mobility particle size spectrometers: harmonization of technical standards and data structure to facilitate high quality long-term observations of atmospheric particle number size distributions, Atmos. Meas. Tech., 5, 657–685, https://doi.org/10.5194/amt-5-657-2012, https://www.atmos-meas-tech.net/5/657/2012/, 2012.